Deformation of adhering elastic tubes

S. Komura[a], K. Tamura, and T. Kato

Department of Chemistry, Faculty of Science, Tokyo Metropolitan University, Tokyo 192-0397, Japan

Abstract. Deformation of an elastic tube adhering onto a substrate due to van der Waals attractive force is investigated by means of numerical minimization and scaling theory. The onset of the deformation is determined by the critical value of $C_b/(\epsilon N^2)$, where C_b is the bending constant, ϵ is the depth of the van der Waals potential, and N is the size of the tube. For a significantly deformed tube, we found a scaling behavior of the bending energy, which is explained within the shell theory.

PACS. 68.35.-p Solid surfaces and solid-solid interfaces: Structure and energetics – 68.55.-a Thin film structure and morphology – 81.07.De Nanotubes

1 Introduction

Carbon nanotubes [1] have attracted great interests due not only to their peculiar structure, but also to the electrical, chemical, and mechanical properties associated with these structures. Examples of the possible applications are such as nanowires or electronic devices. In practice, the electric transport through nanotubes is studied after their deposition on a substrate with which they interact each other. It is known, however, that the resistivity is affected by their elastic deformations. Since there is little control over the alignment and the shape of adsorbed nanotubes, it is crucial to know how they deform on the substrate.

There have been several works which report on the deformations of nanotubes due to van der Waals (vdW) interaction. For example, vdW interaction between adjacent nanotubes can deform them substantially, showing the flattening along the contact region [2]. Multiwalled nanotubes can even fully collapse along their length [3]. Later, the deformations of multiwalled nanotubes on a substrate was investigated using both atomic force microscopy (AFM) [4] and molecular-mechanics simulations [5]. They also showed that the vdW interaction results in the flattening of the tube. More recently, the collapse of a nanotube section due to the surface interaction was observed by using AFM [6].

It is widely known that nanotubes have unique elastic properties such as exceptionally high Young's modulus [7,8]. Bending and buckling of nanotubes [9,10] as well as their axial [11,12] or radial [13] deformations have been experimentally investigated. In general, deformations of nanotube are intimately related to the problem of elastic shell theory [14]. The stretching deformation which accompanies the bending deformation is a first-order effect for a

shell, whereas it is only a second-order effect for a plate. As a result, the shape deformation of a shell is effectively suppressed compared to that of a plate. Such a coupling between the bending and stretching modes was explicitly calculated for a cylindrical polymerized vesicles [15].

In this paper, we investigate the deformation of an elastic nanotube adhering onto a rigid substrate due to vdW attractive interaction both numerically and theoretically. In our model, the equilibrium configuration of the tube is determined according to the competition between the stretching, bending, and vdW energies. The total energy is numerically minimized by using the conjugate gradient method. We have performed the scaling analysis of the minimized energy, and examined how the tube deformation depends on its size and bending constant. The main result of the present work is to show that the combination of the bending constant, the tube size, and the depth of the vdW potential gives a scaling variable both for the onset of the deformation and the total energy. We found two distinct scaling regimes, i.e., "bending regime" and "adhesion regime" which are connected by a crossover region. For a largely deformed tube, the scaling behavior of the bending energy is explained in terms of the shell theory.

2 Model

Consider a cross section of an elastic tube interacting with a rigid substrate as shown in Figure 1. We assume that the axial deformation is uniform along the tube. The elastic tube is modeled by a circular network of N beads connected by harmonic springs. The parallel and the normal directions to the substrate are taken as x- and z-axes, respectively. For the deformations of elastic shells, both the stretching and the bending energies should be taken into

---
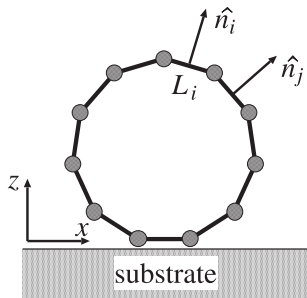[a] e-mail: `komura@comp.metro-u.ac.jp`

Fig. 1. Beads and springs model for an elastic tube adhering onto a substrate. The tube is assumed to deform uniformly along the axial direction. L_i is the length of the i-th spring whose natural length is L_0. $\hat{\boldsymbol{n}}_i$ is the unit normal vector of the i-th spring. Each bead interacts with the substrate through the van der Waals potential energy equation (3).

account [14]. Following the model by Kramer and Witten to simulate crushed elastic manifolds [16], the discretized stretching energy is given by the sum over Hooke's law of each spring:

$$E_{\mathrm{s}} = \sum_i \frac{1}{2} C_{\mathrm{s}} \left(\frac{L_i - L_0}{L_0} \right)^2. \tag{1}$$

Here, C_{s} is the spring constant, L_i is the length of the i-th spring, and L_0 is the natural length of the spring taken here as a constant. The discretized bending energy, on the other hand, is calculated according to [16]

$$E_{\mathrm{b}} = \sum_{\langle ij \rangle} \frac{1}{2} C_{\mathrm{b}} |\hat{\boldsymbol{n}}_i - \hat{\boldsymbol{n}}_j|^2, \tag{2}$$

where C_{b} is the bending constant, $\hat{\boldsymbol{n}}_i$ is the unit normal vector of the i-th spring (see Fig. 1), and the sum is taken over each pair of springs which share a common bead. A spontaneous curvature term is omitted here, which is valid as long as we consider carbon nanotubes composed of graphite sheets. We remark that the same bending energy was used before in the Monte Carlo simulations of two-dimensional vesicles [17].

The adhesion energy of the tube is taken into account through the vdW interaction between each of the bead and the substrate:

$$W = \sum_i \frac{2^{8/3}}{3} \epsilon \left[\left(\frac{\sigma}{z_i} \right)^{12} - \left(\frac{\sigma}{z_i} \right)^3 \right], \tag{3}$$

where z_i is the height of the i-th bead from the substrate. When the adhesion energy per bead is plotted against z_i, ϵ gives the depth of the energy minimum, and the distance corresponding to this minimum is $2^{2/9}\sigma$. The first repulsive term in equation (3) is responsible for the excluded volume interaction which accounts for the fact that the beads cannot penetrate into the substrate. The second term represents the long-ranged attractive interaction between the beads and the substrate [18]. Notice that the inverse cubic dependence of this term results from the

pairwise additivity of the vdW interaction between two atoms [19]. In our model, we have not included the vdW interaction between the different pairs of beads.

The total energy

$$E_{\mathrm{tot}} = E_{\mathrm{s}} + E_{\mathrm{b}} + W \tag{4}$$

is numerically minimized using the conjugate gradient method [20]. As regards the initial condition of the calculation, each bead is located on a circle and each spring length is set to L_0, for which the stretching energy equation (1) is fully relaxed. Since there is no spontaneous curvature, even the undeformed tube costs certain curvature energy. In the present study, we have mainly changed the size N and the bending constant C_{b}.

3 Results and discussions

In our numerical calculation, all the energies and the lengths are scaled by ϵ and σ, respectively. These are the model parameters which appear in the vdW interaction (see Eq. (3)). Then, in addition to the number of beads N, there are three independent dimensionless parameters in the model; C_{s}/ϵ, C_{b}/ϵ, and L_0/σ.

We first show in Figure 2 the sequence of the equilibrated tube configurations as the bending constant is changed from $C_{\mathrm{b}}/\epsilon = 0.01$ to 1000. Here the other dimensionless parameters are fixed to $C_{\mathrm{s}}/\epsilon = 250$, $L_0/\sigma = 200/9 \approx 22.2$, and $N = 100$. In this case, each spring relaxes almost at its natural length. Hence the stretching energy given by equation (1) effectively acts as a constraint of area (circumference) conservation. For a large bending constant such as $C_{\mathrm{b}}/\epsilon = 1000$, the tube hardly deforms in spite of the adhesion, and keeps its circular shape. As the bending constant is reduced to $C_{\mathrm{b}}/\epsilon = 10$, a considerable deformation takes place and the contact area (line) increases significantly. Further decrease of the bending constant results in a configuration obtained such as for $C_{\mathrm{b}}/\epsilon = 0.01$. In this limit, the large curvature is localized at the regions close to the contact line (point), and a significant flattening of the tube is observed.

In order to quantify the deformation of the tube, we use the inertia tensor calculated by

$$I_{\alpha\beta} = \frac{1}{2N^2} \sum_i \sum_j (r_{i,\alpha} - r_{j,\alpha})(r_{i,\beta} - r_{j,\beta}), \tag{5}$$

where $\boldsymbol{r}_i$ is the position of the i-th bead, and $\alpha, \beta = x, z$. Then as a measure of the deformation, we define the so-called anisotropic factor γ:

$$\gamma = \frac{\lambda_1 - \lambda_2}{\lambda_1 + \lambda_2}, \tag{6}$$

where λ_1 and λ_2 ($\lambda_1 > \lambda_2$) are the two eigenvalues of the inertia tensor equation (5). This quantity vanishes when the cross section of the tube is isotropic, but it deviates from zero as soon as the tube starts to undergo any anisotropic deformations. In Figure 3, we have plotted γ
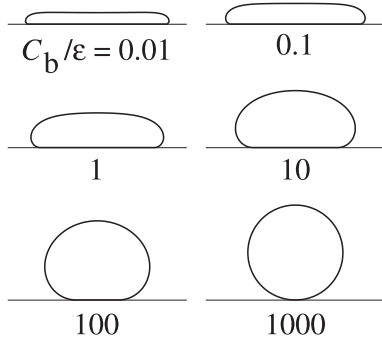
Fig. 2. Equilibrium configurations of the deformed tubes for various values of the scaled bending constant C_b/ϵ when $N = 100$, $C_s/\epsilon = 250$, and $L_0/\sigma = 200/9$.
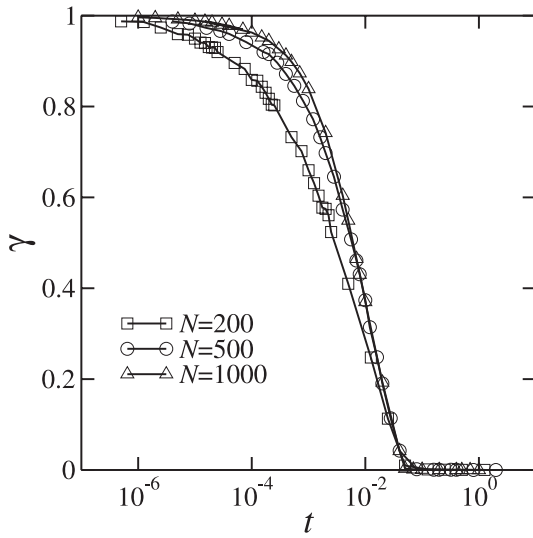

Fig. 3. The anisotropic factor γ defined by equation (6) as a function of $t \equiv C_b/(\epsilon N^2)$ for $N = 200, 500, 1000$. The other parameters are fixed to $C_s/\epsilon = 250$ and $L_0/\sigma = 200/9$. The deformation starts to occur at the critical value $t = t^* \approx 0.05$ irrespective of N.

Fig. 4. The critical value of the deformation t^* as a function of the scaled natural length of the spring L_0/σ for $N = 200$ and $C_s/\epsilon = 250$.
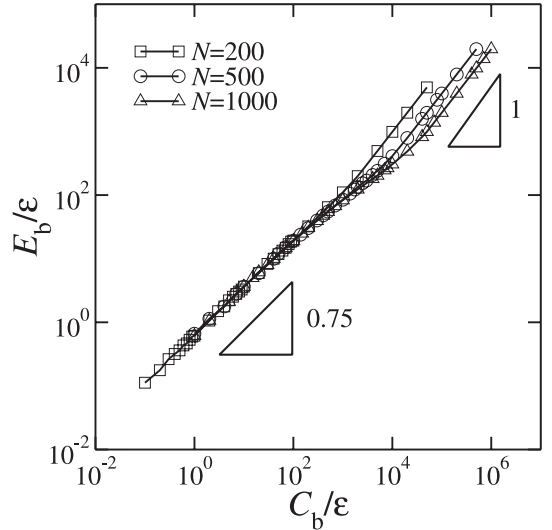
Fig. 5. The minimized scaled bending energy E_b/ϵ as a function of the scaled bending constant C_b/ϵ for $N = 200, 500, 1000$. The other parameters are fixed to $C_s/\epsilon = 250$ and $L_0/\sigma = 200/9$. There are two scaling behaviors; $E_b/\epsilon \sim (C_b/\epsilon)/N$ and $E_b/\epsilon \sim (C_b/\epsilon)^{0.75}$ for large and small C_b/ϵ, respectively.

as a function of the newly defined variable $t \equiv C_b/(\epsilon N^2)$ for three different tube sizes, i.e., $N = 200, 500, 1000$. The physical meaning of this scaling variable will be discussed later. With this combination of variables, we see a clear transition at $t^* \approx 0.05$ between the undeformed and the deformed tubes. This transition looks a continuous second-order transition while the buckling phenomena does not occur. We stress here that the critical value t^* does not depend on the tube size N. For a fixed spring constant C_s, however, we found that t^* is weakly dependent on the natural length of the spring L_0. This result is shown in Figure 4 where we plotted t^* as a function of L_0/σ for $N = 200$. We see that t^* decreases almost linearly with increasing L_0, although it is a rather weak dependence. These results imply that tubes with larger N and/or smaller L_0 are more flexible against the deformation.

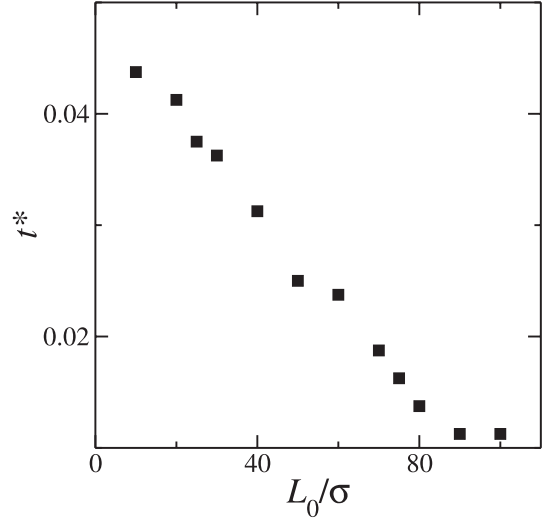For an almost undeformed tube, its bending energy can be readily estimated, since the curvature is uniformly distributed on the circle. In such a case, the radius of curvature is proportional to N, and the total bending energy equation (2) becomes simply

$$E_b \sim N \left(\frac{C_b}{N^2} \right) \sim \frac{C_b}{N}, \tag{7}$$

or

$$\frac{E_b}{\epsilon} \sim \frac{(C_b/\epsilon)}{N}. \tag{8}$$

This linear relation between E_b/ϵ and C_b/ϵ in the undeformed region can be checked in Figure 5. The fact that the data of E_b/ϵ splits into three different lines reflects
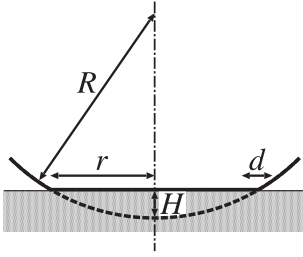
Fig. 6. Various notations characterizing the tube deformation due to the adhesion.

a size dependence on $1/N$ in equation (8) for large C_b/ϵ. Since $t = E_b/(\epsilon N)$ holds in this regime, the critical value of t in Figure 3 can be understood as the value at which the scaled bending energy per bead $E_b/(\epsilon N)$ becomes $t^* \approx 0.05$. For small C_b/ϵ, on the other hand, all the data collapse on a single straight line regardless of the tube size N. In this region of strong deformation, we observe a non-trivial scaling behavior, i.e., $E_b/\epsilon \sim (C_b/\epsilon)^{0.75}$, which can be understood within the shell theory [14] as explained below.

When a tube of radius R is largely deformed on a substrate (see $C_b/\epsilon = 1$ in Fig. 2), a contact area of width $2r$ develops as shown in Figure 6. For such a deformation, the elastic energy is localized in the two parallel straight strips near the edge of the bulge. Let us denote the width of the bending strip by d. Then the displacement of points in the bending strip ζ can be geometrically determined as $\zeta \sim dr/R$. The associated strain and the curvature due to the displacement ζ are given by ζ/R and ζ/d^2, respectively [14]. One can then show that the relevant stretching and bending energies per unit area scale as

$$\left(\frac{C_s}{L_0^2}\right)\left(\frac{\zeta}{R}\right)^2 \sim \left(\frac{C_s}{L_0^2}\right)\frac{d^2 r^2}{R^4}, \qquad (9)$$

and

$$C_b\left(\frac{\zeta}{d^2}\right)^2 \sim C_b\frac{r^2}{d^2 R^2}, \qquad (10)$$

respectively. These energies per unit area are multiplied by the width of the bending strip d to obtain the following energies per unit length of the tube:

$$E_s \sim \left(\frac{C_s}{L_0^2}\right)\frac{d^3 r^2}{R^4}, \qquad (11)$$

$$E_b \sim C_b\frac{r^2}{dR^2}. \qquad (12)$$

Minimizing the sum of these energies with respect to d, the width of the bending strip is obtained as

$$d \sim \left(\frac{C_b L_0^2}{C_s}\right)^{1/4} R^{1/2}. \qquad (13)$$

By putting back this relation into equation (12), we find that the minimized total bending energy per unit length scales as

$$E_b \sim \left(\frac{C_s}{L_0^2}\right)^{1/4} C_b^{3/4}\frac{r^2}{R^{5/2}} \sim \left(\frac{C_s}{L_0^2}\right)^{1/4} C_b^{3/4}\frac{H}{R^{3/2}}. \qquad (14)$$
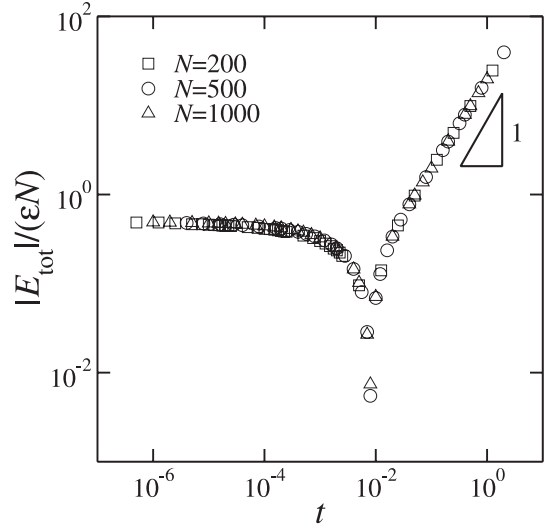

Fig. 7. The absolute value of the total energy per bead $|E_{tot}|/(\epsilon N)$ as a function of the scaling variable $t = C_b/(\epsilon N^2)$. The parameters are fixed to $C_s/\epsilon = 250$ and $L_0/\sigma = 200/9$. The scaling $E_{tot}/(\epsilon N) \sim t$ holds in the "bending regime", whereas $E_{tot}/(\epsilon N)$ asymptotically approaches to -1 in the "adhesion regime".

In the last expression, we have used the relation $r \sim (HR)^{1/2}$ [14], where H is the depth of the bulge (see Fig. 6). For a fixed size of tube, the obtained scaling relation in equation (14) accounts for the behavior of $E_b/\epsilon \sim (C_b/\epsilon)^{0.75}$ in Figure 5. We comment here that the corresponding expression of the bending energy for a spherical shell has similar dependences on C_s and C_b, but different dependences on H and R [14,21]. Moreover, the scaling relation in equation (14) is valid as long as H is fixed and given.

In Figure 7, we have plotted the scaled absolute value of the total energy per bead $|E_{tot}|/(\epsilon N)$ as a function of $t = C_b/(\epsilon N^2)$ for three different tube sizes as before. Notice that E_{tot} can take negative value due to the vdW interaction when the tube is strongly adsorbed. It is remarkable that all the data collapse onto a single curve irrespective of the tube size N. When the tube is undeformed for large t, the bending energy is the main contribution to the total energy. As discussed before, we have the scaling behavior

$$\frac{E_{tot}}{\epsilon N} \sim \frac{E_b}{\epsilon N} \sim \frac{C_b}{\epsilon N^2} \sim t, \qquad (15)$$

in this regime (see Eq. (8)). This relation is strictly satisfied in Figure 7 for $t > t^*$ where we call as the "bending regime". For small t, on the other hand, $|E_{tot}|/(\epsilon N)$ asymptotically approaches to a constant (unity). This behavior is consistent with the fact that most of the beads are strongly adsorbed on the substrate when t is small. We remind that the depth of the potential minimum in the vdW adhesion energy per bead (see Eq. (3)) is -1 in unit of ϵ. Hence we call this small t limit as the "adhesion regime". These two regimes are connected by a crossover region in which the bending and the adhesion energies compete with each other.

Here we discuss the physical meaning of the scaling variable t. Consider the case where the indentation H in equation (14) is caused by the adhesion. The corresponding energy gain per unit length of the tube is

$$E_{\mathrm{a}} \sim wr \sim w(HR)^{1/2}, \qquad (16)$$

where w is the vdW energy per unit area. In reference [21], we showed that w can be approximately given by $w \sim A/(12\pi D^2)$, where A is the Hamaker constant and D is an atomic cutoff for the vdW interaction. If the deformations are driven by vdW adhesion, the adhesion energy E_{a} is expected to balance with the bending energy E_{b} in equation (14). By setting $E_{\mathrm{a}} \sim E_{\mathrm{b}}$, we arrive at the estimate for indentation H:

$$H \sim \frac{L_0 w^2 R^4}{C_{\mathrm{s}}^{1/2} C_{\mathrm{b}}^{3/2}}, \qquad (17)$$

for given w and R. Since the tube radius R is the only length scale in the problem, we replace H by R and obtain the relation:

$$\frac{C_{\mathrm{b}}}{R^2} \sim \frac{L_0^{2/3} w^{4/3}}{C_{\mathrm{s}}^{1/3}}. \qquad (18)$$

This result suggests that $C_{\mathrm{b}}/(\epsilon R^2) \sim C_{\mathrm{b}}/(\epsilon N^2) \sim t$ can be the dimensionless scaling variable for any deformation because the right hand side does not depend on R.

We note here that the upper part of the tube is not a part of a circle with radius R especially when the tube is strongly deformed as shown in Figure 2. Since the spontaneous curvature is not considered in our model, the flattening of the tube reduces the bending energy. In such a case, the bending energy is localized at the regions close to the contact line, and the above analysis becomes more accurate.

We finally comment that the present work is related to the problem of vesicle adhesion which was considered by Seifert and Lipowsky [22]. For spherical vesicles, various axisymmetric shapes were calculated by minimizing the sum of the bending and the adhesion energies under the constraint of constant area or volume. Apart from their shapes, one of the major differences between the nanotubes and the vesicles is that the vesicles do not support any stretching energy. Moreover, the vesicles feel the adhesion potential only when they are in contact with the substrate, whereas the long-ranged interaction acts on all of the beads in our model.

4 Conclusion

We have investigated the deformation of the elastic tube adhering onto the substrate by using the conjugate gradient method and the scaling argument. We found that the onset of the deformation and the total energy per bead exhibit universal behaviors when $C_{\mathrm{b}}/(\epsilon N^2)$ is chosen as the scaling variable. Further studies such as a tube with a spontaneous curvature, or deformation of a spherical shell are under progress.

References

1. S. Iijima, Nature **354**, 56 (1991)
2. R.S. Ruoff, J. Tersoff, D.C. Lorents, S. Subramoney, B. Chan, Nature **364**, 514 (1993)
3. N.G. Chopra, L.X. Benedict, V.H. Crespi, M.L. Cohen, S.G. Louie, A. Zettl, Nature **377**, 135 (1995)
4. T. Hertel, R. Martel, P. Avouris, J. Phys. Chem. B **102**, 910 (1998)
5. T. Hertel, R.E. Walkup, P. Avouris, Phys. Rev. B **58**, 13870 (1998)
6. M.-F. Yu, T. Kowalewski, R.S. Ruoff, Phys. Rev. Lett. **86**, 87 (2001)
7. M.M.J. Treacy, T.W. Ebbesen, J.M. Gibson, Nature **381**, 678 (1996)
8. E. Hernández, C. Goze, P. Bernier, A. Rubio, Phys. Rev. Lett. **80**, 4502 (1998)
9. M.R. Falvo, G.J. Clary, R.M. Taylor, V. Chi, F.P. Brooks, S. Washburn, R. Superfine, Nature **389**, 582 (1997)
10. E.W. Wong, P.E. Sheehan, C.M. Lieber, Science **277**, 1971 (1997)
11. M.-F. Yu, O. Lourie, M.J. Dyer, K. Moloni, T.F. Kelly, R.S. Ruoff, Science **287**, 637 (2000)
12. T. Ozaki, Y. Iwasa, T. Mitani, Phys. Rev. Lett. **84**, 1712 (2000)
13. M.-F. Yu, T. Kowalewski, R.S. Ruoff, Phys. Rev. Lett. **85**, 1456 (2000)
14. L.D. Landau, E.M. Lifshitz, *Theory of Elasticity* (Pergamon, Oxford, 1986)
15. S. Komura, R. Lipowsky, J. Phys. II France **2**, 1563 (1992)
16. E.M. Kramer, T.A. Witten, Phys. Rev. Lett. **78**, 1303 (1997)
17. S. Leibler, R.R.P. Singh, M.E. Fisher, Phys. Rev. Lett. **59**, 1989 (1987)
18. J.N. Israelachivili, *Intermolecular and Surface Forces* (Academic, London, 1991)
19. S.A. Safran, *Statistical Thermodynamics of Surface, Interfaces, and Membranes* (Addison-Wesley, New York, 1994).
20. W.H. Press et al., *Numerical Recipes* (Cambridge University, New York, 1989)
21. U.S. Schwarz, S. Komura, S.A. Safran, Europhys. Lett. **50**, 762 (2000)
22. U. Seifert, R. Lipowsky, Phys. Rev. A **42**, 4768 (1990)